International Journal of GEOMATE, March, 2021, Vol.20, Issue 79, pp. 74-81
ISSN: 2186-2982 (P), 2186-2990 (O), Japan, DOI: https://doi.org/10.21660/2021.79.GX192
Geotechnique, Construction Materials and Environment

# EVALUATION OF EARTHQUAKE-INDUCED SLOPE FAILURE DISTRIBUTION USING THE AHP METHOD AND GIS

*Masanori Kohno[1,2] and Yusuke Ono[1,2]

[1]Faculty of Engineering, Tottori University, Japan
[2]Center for Regional Management and Safety Engineering, Tottori University, Japan

*Corresponding Author, Received: 15 Jun. 2020, Revised: 05 Jan. 2021, Accepted: 28 Jan. 2021

**ABSTRACT:** Landslides or slope failures are often caused by earthquakes. The 2018 Hokkaido Eastern Iburi Earthquake and the 2016 Kumamoto Earthquakes in Japan caused many slope failures that were distributed both widely and densely. This study proposes an earthquake-induced slope failure hazard mapping method that uses the analytic hierarchy process (AHP) and a geographic information system (GIS) for specific districts, the Atsuma district in Hokkaido and Minamiaso district in Kumamoto. The earthquake-induced slope failure hazard assessment system used here is based on the landslide distribution (NIED catalog, Japan), which includes tens of thousands of locations in the Atsuma and Minamiaso districts. We considered the relationships between landslide distribution and landslide hazard factors (elevation, slope angle, slope type, catchment degree, geology, and vegetation). These relations were introduced to pairwise comparisons of factors in the AHP method. The AHP method was applied to evaluate the slope failure hazard rank. An earthquake-induced slope failure hazard map was created based on slope failure hazard ranks of I–V. As a result, slope angle, slope type, and catchment degree were found to exert maximum effects on slope failure distribution due to earthquakes in both the Atsuma district in Hokkaido and the Minamiaso district in Kumamoto. The two earthquake-induced slope failure distributions are almost consistent with the slope failure hazard rank. These results provide a practical method for evaluating earthquake-induced slope failure hazards.

*Keywords: Earthquake-induced slope failure, AHP method, GIS, Landslide distribution*

## 1. INTRODUCTION

Alteration by volcanic hydrothermal systems and the formation of crushing and weathering zones have occurred widely throughout the Pacific region over geologic time. As a result of these geologic processes, fragile geological features and steep topography can be found on the Earth's surface. Landslides or slope failures are often caused by earthquakes. In Japan, the 2018 Hokkaido Eastern Iburi Earthquake [1, 2] and 2016 Kumamoto Earthquakes [3, 4] caused many slope failures that occurred over a wide area and were also densely clustered. (Fig. 1 shows plots of slope failure and landslide distributions that are based on GSI [5] and NIED [6, 7]). Predicting the risk of slope failure and establishing appropriate preventative measures is extremely important. However, implementing preventive measures in all locations that are at risk of slope failure is financially challenging. Therefore, it is necessary to identify slopes with a high risk of collapse and implement investigative countermeasures based on the level of priority. In such cases, one of the first items to pay attention to is topography. In recent years, aerial video surveys using drones (UAV) [8–12] have attracted attention and demonstrated their advantages in terms of time and cost when conducting wide-area topographic surveys. However, there are still some high hurdles to clear, such as Aviation Law, Radio Law, and ordinances. Therefore, as another approach, if the slope failure risk area during an earthquake can be objectively and easily extracted from data that is easily available and highly versatile, this will be very useful. Previous studies have attempted to map slope failure hazards using various techniques. More recently, many researchers and engineers have performed landslide hazard assessment using geographic information systems (GIS) [13–19]. Furthermore, some researchers reported a method of evaluating slope failure hazard using the analytic hierarchy process (AHP) method [16, 19–28]. This method does not require the subjective and empirical judgment of researchers or engineers. However, since the methods that use the AHP model are limited to evaluation within the landslide topography, the method used in this study mainly considers re-active-type landslides. This method was developed by several skilled engineers who have conducted landslide surveys over many years. However, it largely depends on the subjective and empirical judgments of the evaluators, which requires time and a high level of skill because the evaluation factors are subdivided.

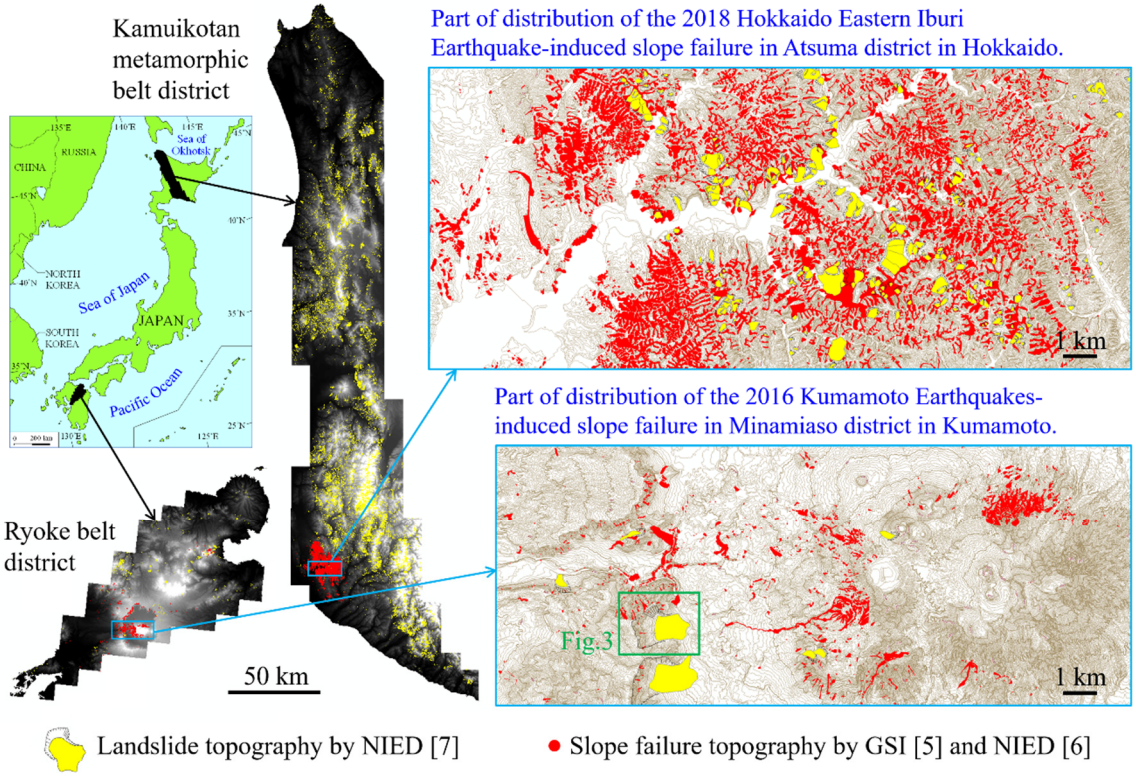


Fig.1 Location of the study area (Kamuikotan metamorphic belt and Ryoke belt districts) and distribution map of the landslides in the Atsuma and Minamiaso districts.

This study proposes an earthquake-induced slope failure hazard mapping method using the AHP method and GIS for two specific areas: the Atsuma district in Hokkaido and Minamiaso district in Kumamoto. The Atsuma and Minamiaso districts are within the inner Kamuikotan metamorphic belt and Ryoke belt [29], respectively. Hence, the AHP and GIS analytical ranges in this study are limited to these geological belt districts (Fig. 1).

## 2. METHODOLOGY

The AHP, which is a decision-making method developed by Saaty [30], is an analytical method that determines the importance weight of evaluation factors based on paired comparison. When setting the analysis target area by GIS, geological or administrative division can be considered. However, in this study, the areas examined are the Kamuikotan metamorphic belt and the Ryoke belt (Fig. 1), based on the geotectonic subdivision [29] of Japan. Each area includes the slope failure distribution area due to the 2018 Hokkaido Eastern Iburi Earthquake or the 2016 Kumamoto Earthquakes. First, the relationship between the landslide topography area and the evaluation factors/elements area (i.e., the area ratio of the two) was statistically clarified based on the landslide distribution map [7] (Fig. 1) of the Kamuikotan metamorphic belt and the

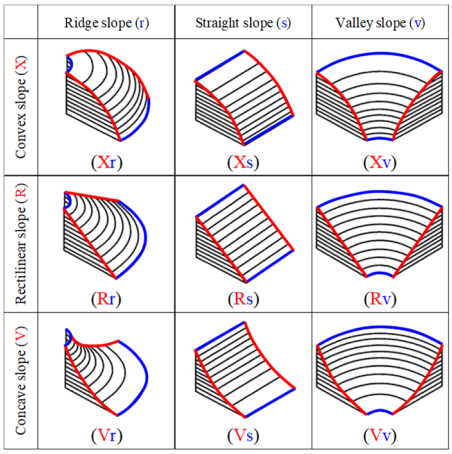


Fig.2 Basic classification of slope type (Based on Suzuki [34]).

Ryoke belt. In this study, there are six evaluation factors related to the level of risk of landslides based on the AHP as follows: elevation, slope angle, slope type, catchment degree, geology, and vegetation. The topographic, geological, and vegetation data used in this study are the Digital Elevation Model (DEM10B) by GSI [31], Seamless Digital Geological Map of Japan (1:200,000) by the Geological Survey of Japan [32], and the Natural Environmental Information GIS by the Biodiversity Center of Japan [33]. The slope type can be divided into 9 specific types (Fig. 2), based on those described by Suzuki [34]. To

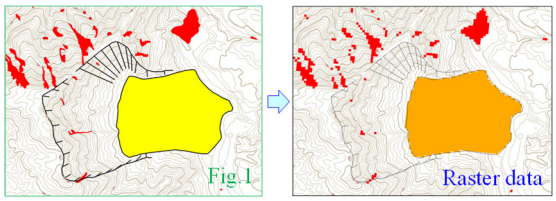


Fig.3 Conversion of landslide topography to raster data (20 m × 20 m cell).

calculate the catchment degree, Terrain Analysis Using Digital Elevation Models [35] is incorporated into GIS. Hierarchy level 2 is classified as follows. Kamuikotan metamorphic belt: the elevation is divided into 9 divisions ranging from 0 to 1800 m at 200 m intervals, the slope angle is divided into 8 divisions ranging from 0 to 80° at 10° intervals, the slope type is divided into 9 divisions based on Fig. 2, the catchment degree includes 5 divisions from 20 to 7271.58, and geology and vegetation are divided into 14 and 9 divisions based on the data legend [32, 33], respectively; Ryoke belt: the elevation is divided into 9 divisions ranging from 0 to 1800 m in 200 m intervals, the slope angle is divided into 9 divisions ranging from 0 to 80° in 10° intervals, the slope type is divide into 9 divisions based on Fig. 2, the catchment degree includes 5 divisions from 20 to 3728.43, and geology and vegetation are divided into 15 and 7 divisions based on the data legend [32, 33], respectively. As shown in Fig. 3, this study used raster data from the landslide body.

A hierarchical system for landslide risk assessment was constructed based on these sets of evaluation factors. Using this hierarchical structure, the importance weight of each element is first calculated, and then the importance weight between the higher evaluation factors is calculated. Saaty [30] gave a nine-point scale. Equal importance is 1; moderate importance is 3; strong importance is 5; very strong importance is 7; and absolute importance is 9. 2, 4, 6, and 8 are assigned to elements with intermediate importance weights. Therefore, the subjective and empirical judgment of the engineer is indispensable when using the AHP standard nine-point scale. Therefore, in this study, the importance weights are calculated by introducing the statistical survey results of the relationship between the landslide topography distribution and the factors in the paired comparison. Landslide hazard mapping is conducted by ranking the landslide risk for each evaluation factor based on the estimated importance weight of each hierarchy and totaling the landslide risk scores applicable to each evaluation factor on each slope using GIS. Finally, evaluation factors with maximum impact were identified and their suitability was examined by

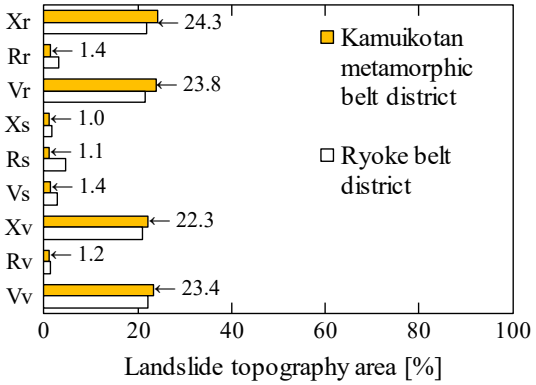


Fig.4 One example of the relationship between landslide distribution and evaluation factors (e.g., slope type). Abbreviations in this figure correspond to Fig. 2.

| Level 2 | Xr | Rr | Vr | Xs | Rs | Vs | Xv | Rv | Vv | weight |
|---|---|---|---|---|---|---|---|---|---|---|
| Xr | 1 | 17.36 | 1.02 | 24.30 | 22.09 | 16.20 | 1.09 | 20.25 | 1.04 | 24.29 |
| Rr | 0.06 | 1 | 0.06 | 1.40 | 1.27 | 0.93 | 0.06 | 1.17 | 0.06 | 1.43 |
| Vr | 0.98 | 17.00 | 1 | 23.80 | 21.64 | 15.87 | 1.07 | 19.83 | 1.02 | 23.85 |
| Xs | 0.04 | 0.71 | 0.04 | 1 | 0.91 | 0.67 | 0.04 | 0.83 | 0.04 | 1.02 |
| Rs | 0.05 | 0.79 | 0.05 | 1.10 | 1 | 0.73 | 0.05 | 0.92 | 0.05 | 1.10 |
| Vs | 0.06 | 1.07 | 0.06 | 1.50 | 1.36 | 1 | 0.07 | 1.25 | 0.06 | 1.46 |
| Xv | 0.92 | 15.93 | 0.94 | 22.30 | 20.27 | 14.87 | 1 | 18.58 | 0.95 | 22.29 |
| Rv | 0.05 | 0.86 | 0.05 | 1.20 | 1.09 | 0.80 | 0.05 | 1 | 0.05 | 1.19 |
| Vv | 0.96 | 16.71 | 0.98 | 23.40 | 21.27 | 15.60 | 1.05 | 19.50 | 1 | 23.37 |

Fig.5 One example of pairwise comparisons of evaluation factors (e.g., slope type, Kamuikotan metamorphic belt) in hierarchy level 2. Abbreviations in this figure correspond to Fig. 2.

| Hierarchy level 1 | | A | B | C | D | E | F | weight |
|---|---|---|---|---|---|---|---|---|
| A | Elevation | 1 | 0.67 | 0.60 | 1.80 | 0.71 | 0.83 | 13.64 |
| B | Slope angle | 1.50 | 1 | 0.89 | 2.70 | 1.07 | 1.25 | 20.43 |
| C | Slope type | 1.68 | 1.12 | 1 | 3.02 | 1.20 | 1.39 | 22.87 |
| D | Catchment degree | 0.55 | 0.37 | 0.33 | 1 | 0.40 | 0.46 | 7.57 |
| E | Geology | 1.40 | 0.93 | 0.83 | 2.52 | 1 | 1.16 | 19.09 |
| F | Vegetation | 1.20 | 0.80 | 0.72 | 2.17 | 0.86 | 1 | 16.40 |

Fig.6 One example of pairwise comparisons of evaluation factors in hierarchy level 1 (e.g., Kamuikotan metamorphic belt).

comparing the composed landslide hazard map with the slope failure distribution due to earthquakes.

## 3. EARTHQUAKE-INDUCED SLOPE FAILURE HAZARD MAPPING

### 3.1 Pairwise Comparisons of Factors in Hierarchy Levels 1 and 2

As an example, the relationship between landslide distribution and factor (slope type) and the pairwise comparisons of factor (slope type) in hierarchy level 2 are shown in Figs. 4 and 5. Slope failures are densely distributed in convex-ridge,

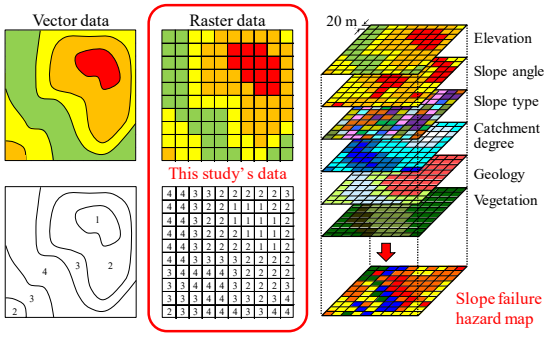


Fig.7 Overlaying of the GIS model's raster data.

concave-ridge, convex-valley, and concave-valley slope type areas. According to these results, it is thought that earthquake-linked slope failure is closely related to slope type. As mentioned above, the ratio of the slope failure area and factors in hierarchy level 2 from the relationship obtained in Fig. 4 were used as the numerical value of the pairwise comparisons. Taking the slope type of the Kamuikotan metamorphic belt district as an example, the value of the pairwise comparison between Xr (Fig. 4: 24.3%) and Rr (Fig. 4: 1.4%) in Fig. 5 is 24.3 / 1.4 = 17.36, and the pairwise comparison between Rr and Xr is the reciprocal (0.06). It can be seen that the order of importance weights (Fig. 5) corresponds to Fig. 4. The weight of hierarchy level 1 (Fig. 6) is calculated based on Kohno et al. [28]. The landslide hazard score p is calculated using the AHP hierarchy weight and is given by Eq. (1) [28].

$$p = \frac{W_1 W_2}{W_{2\mathrm{MAX}}} \times 100 \qquad (1)$$

where $W_1$ is the weight of hierarchy level 1, $W_2$ is the weight of hierarchy level 2, and $W_{2\mathrm{MAX}}$ is the highest weight of hierarchy level 2. Landslide hazard mapping was performed on the basis of the hazard rank classified from I to V, with the total landslide risk score corresponding to each evaluation factor (overlaid using GIS; Fig. 7) for a certain slope (raster data: 20 m × 20 m cell) set as the total landslide risk score $P$. If the total score $P$ is large, the risk of landslide is high, and if the score is small, the risk is low.

### 3.2 Landslide Hazard Mapping based on 6 Factors

An example of a landslide hazard map in the Kamuikotan metamorphic belt and Ryoke belt districts is shown in Fig. 8. In these examples, it can be seen that the hazard rank III and IV distribution areas occupy most of the slope failure distribution area. The relationship between

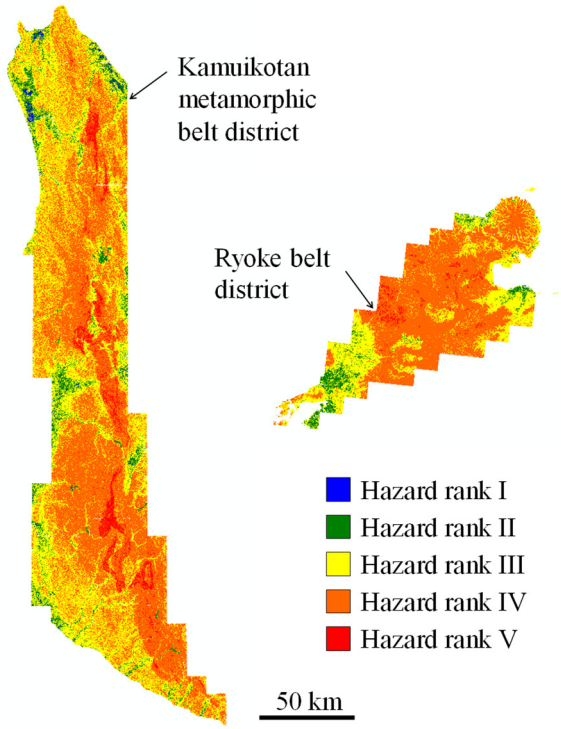


Fig.8 One example of a landslide hazard map in the Kamuikotan metamorphic belt and Ryoke belt districts.

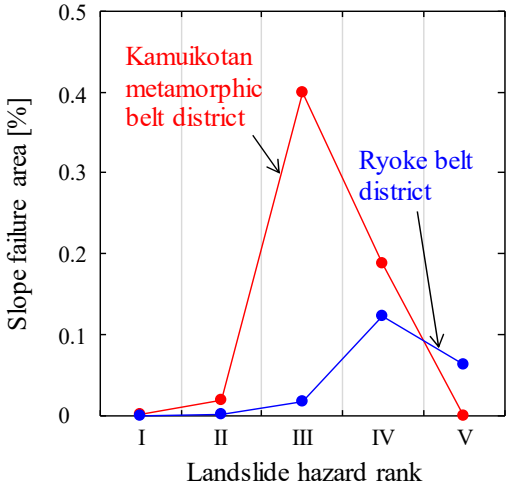


Fig.9 Relationship between landslide hazard rank and slope failure distributions in the landslide hazard map shown in Fig. 8.

landslide hazard rank and slope failure area based on these maps is shown in Fig. 9. The slope failure area peaked at hazard rank III and decreased in the hazard rank IV and V distribution areas. The composed landslide hazard map clearly shows that landslides did not necessarily occur in areas with high landslide risk. Therefore, the landslide hazard map created using this method does not necessarily represent the slope failure distribution caused by earthquakes.

### 3.3 Landslide Hazard Mapping based on Topographical Factors

Thus, we investigated the evaluation factors that had the maximum effect on slope failure. This method calculates the landslide risk score by positioning the importance of evaluation factors in hierarchy level 1 as 99.9, and the importance of other evaluation factors as 0.02, and performs landslide hazard mapping accordingly. As a result, the relationship between landslide hazard rank and cumulative relative frequency is shown in Fig. 10. As shown in this figure, in terms of elevation and geology, slope failures of 80% or more have already occurred in the distribution area where the landslide hazard rank is considered to be relatively low for I and II. Therefore, the involvement of elevation and geology in slope failure distribution is not very large. In general, it is well known that there is a close relationship between slope failure and geology. However, the degree of influence did not appear in the slope failure distribution that occurred in the same geological environment. For the other factors, the cumulative relative frequency of the slope failure area tends to increase as the hazard rank increases. All three factors (inclination slope angle, slope type, and catchment degree) other than vegetation are topographical predisposing items. Therefore, slope angle, slope type, and catchment degree were found to exert maximum effects on slope failure distribution due to earthquakes in both districts. Therefore, we performed landslide hazard mapping by employing only slope angle, slope type, and catchment degree as evaluation factors and investigated the relationship between the composed hazard map and the slope failure distribution. The relationship between landslide hazard rank and slope failure distributions in the landslide hazard map based on slope angle, slope type, and catchment degree is shown in Fig. 11. With increasing landslide hazard rank, the slope failure area also demonstrate an increasing trend. There was significant correspondence between all case hazard ranks and slope failure distribution. Needless to say, this is because landslide hazard mapping was performed by collecting and setting only those factors closely related to the slope failure distribution. Therefore, assessing the slope failure hazard using the three factors of inclination slope angle, slope type, and catchment degree allows areas with a high risk of slope failure due to a sudden phenomenon such as an earthquake to be identified in advance, and this can be an effective method to achieve that goal.

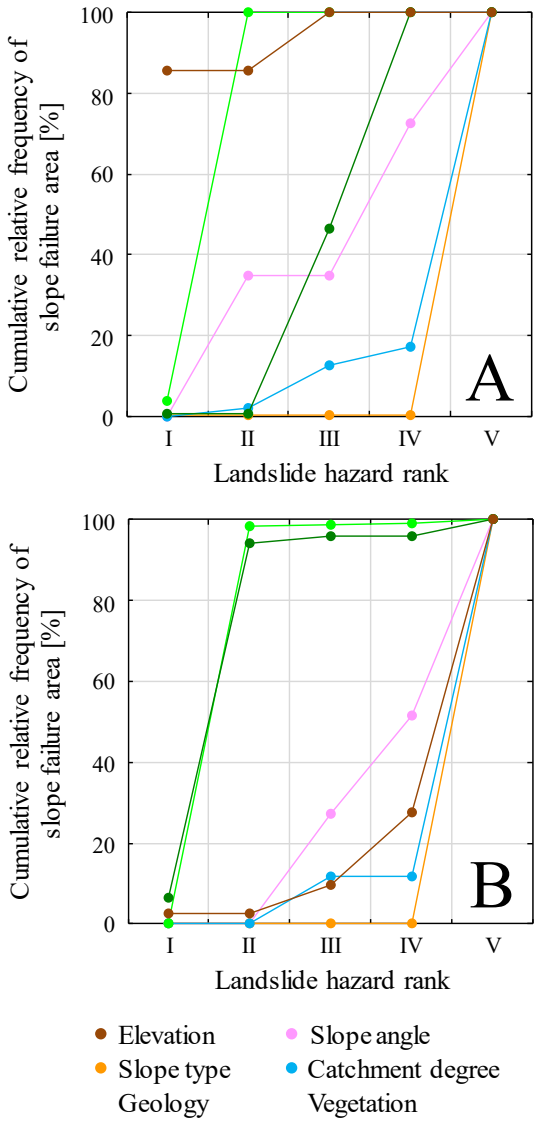


Fig.10 Relationship between landslide hazard rank and cumulative relative frequency. Each weight of the hierarchy level is 99.9%. A: Kamuikotan metamorphic belt district, B: Ryoke belt district.

## 4. CONCLUSION

This study proposed an earthquake-induced slope failure hazard mapping method using the AHP and a GIS for two specific districts: the Kamuikotan metamorphic belt and the Ryoke belt.

In this study, the importance weights were calculated by introducing the statistical survey results for the relationship between the landslide topography distribution and the factors in the paired comparison in AHP. The AHP method was applied to evaluate the slope failure hazard rank. An earthquake-induced slope failure hazard map was created based on slope failure hazard ranks of I–V. As a result, slope angle, slope type, and catchment degree were found to exert maximum effects on slope failure distribution due to earthquakes in both the Atsuma district in Hokkaido and the Minamiaso district in Kumamoto. There was significant correspondence

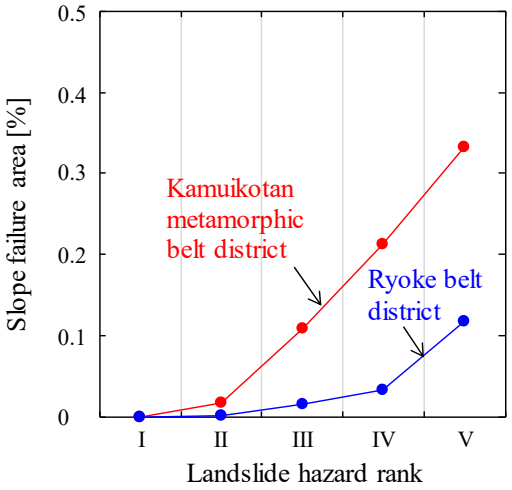


Fig.11 Relationship between landslide hazard rank and slope failure distributions in the landslide hazard map based on slope angle, slope type, and catchment degree in the Kamuikotan metamorphic belt and Ryoke belt districts.

between all hazard ranks and the two earthquake-induced slope failure distributions.

This study identified the factors that are related to landslides, determined the relationship between the factors and landslides, and provided a method to predict future landslide hazards based on this relationship. Our methods provide a practical method for evaluating earthquake-induced slope failure hazards. In order to further develop this method of evaluating landslide hazards in the future, we will apply our method to various districts.

## 5. ACKNOWLEDGMENTS

This work was partly supported by a research grant (Principal Investigator: Masanori Kohno) of the Japan Society of Erosion Control Engineering, research grant (Principal Investigator: Masanori Kohno) of Chugoku Construction Public utility Association, and Grants-in-Aid for Scientific Research "KAKENHI" (Grant Number 18H01523, Principal Investigator: Yusuke Ono) of the Japanese Society for the Promotion of Sciences (JSPS). This support is gratefully acknowledged.

## 6. REFERENCES

[1] Earthquake Research Committee, The Headquarters for Earthquake Research Promotion, Evaluation of the 2018 Hokkaido Eastern Iburi Earthquake (October 12, 2018), Monthly Reports on Evaluation of Seismic Activities in Japan, 2018.

[2] Japan Meteorological Agency, The 2018 Hokkaido Eastern Iburi Earthquake -Portal-, https://www.jma.go.jp/jma/en/2018_Hokkaido_Eastern_Iburi_Earthquake/index.html, Accessed April 2020.

[3] Earthquake Research Committee, The Headquarters for Earthquake Research Promotion, Evaluation of the 2016 Kumamoto Earthquakes (May 13, 2016), Monthly Reports on Evaluation of Seismic Activities in Japan, 2016.

[4] Japan Meteorological Agency, The 2016 Kumamoto Earthquake -Portal-, https://www.jma.go.jp/jma/en/2016_Kumamoto_Earthquake/2016_Kumamoto_Earthquake.html, Accessed April 2020.

[5] Geospatial Information Authority of Japan (GSI), Landslide distribution map by the 2018 Hokkaido Eastern Iburi Earthquake, 2018, https://www.gsi.go.jp/BOUSAI/H30-hokkaido iburi-east-earthquake-index.html (in Japanese), Accessed April 2020.

[6] National Research Institute for Earth Science and Disaster Resilience (NIED), Landslide distribution map by the 2016 Kumamoto Earthquake, 2016, https://www.bosai.go.jp/mizu/dosha.html (in Japanese), Accessed April 2020.

[7] National Research Institute for Earth Science and Disaster Resilience (NIED), Digital archive for Landslide Distribution Maps, http://dil-opac.bosai.go.jp/publication/nied_tech_note/landslidemap/gis.html (in Japanese), Accessed April 2020.

[8] Tanaka R., Okabayashi T., Toyama I. and Yamamoto K., A proposal of topographical survey by using motion video taken from drone, Proceedings of 8th Symposium on Sediment-Related Disasters, pp. 61-66. 2016 (in Japanese).

[9] Lindner G., Schraml K. Mansberger R. and Hübl J., UAV monitoring and documentation of a large landslide, Applied Geomatics, Vol. 8, 2016, pp. 1-11.

[10] Niethammer U., James M.R., Rothmund S., Travelletti J. and Joswig M., UAV-based remote sensing of the Super-Sauze landslide: Evaluation and results, Engineering Geology, Vol. 128, Issue 9, 2012, pp. 2-11.

[11] Yamamura M., Uchiyama S. and Kumai N., Application of sequential monitoring by UAV-SfM for evaluating deposits of the sediment control dam, Landslides – Journal of the Japan Landslide Society, Vol. 53, Issue 6, 2016, pp. 235-239 (in Japanese).

[12] Watanabe T., Yamasaki S. and Kameda J., Training course of the method to make a digital surface model by using Unmanned Aerial Vehicle (UAV) and high-precision Global Navigation Satellite System (GNSS), The Journal of the Geological Society of

Japan, Vol. 124, Issue 8, 2018, pp. 643-649 (in Japanese).
[13] Nagata H., Sakaguchi T. and Kojima S., Analysis of topographic and geologic factors in unstable slope distribution using GIS, Journal of the Japan Society of Engineering Geology, Vol. 46, Issue 6, 2006, pp. 320-330 (in Japanese).
[14] Zhou G., Yokota N., Cheng G. and Kitazono Y., An advanced slope failure hazard mapping method by combing GIS and Hayashi's quantification methods theory, Journal of the Japan Society of Engineering Geology, Vol. 49, Issue 1, 2008, pp. 2-12 (in Japanese).
[15] Wang L., Sawada K. and Moriguchi S., Landslide susceptibility mapping by using logistic regression model with neighborhood analysis: A case study in Mizunami city, International Journal of GEOMATE, Vol. 1, Issue 2, 2011, pp. 99-104.
[16] Phukon P., Chetia D. and Das P., Landslide susceptibility assessment in the Guwahati City, Assam using Analytic Hierarchy Process (AHP) and Geographic Information System (GIS), International Journal of Computer Applications in Engineering Sciences, Vol. 2, Issue 1, 2012, pp. 1-6.
[17] Hamasaki E., Higaki D. and Hayashi K., Buffer movement analysis and blunder probability analysis for GIS-based landslide susceptibility mapping -A case study of the 2008 Iwate-Miyagi Nairiku Earthquake, Japan-, Landslides – Journal of the Japan Landslide Society, Vol. 52, Issue 2, 2015, pp. 51-59 (in Japanese).
[18] Priyono K.D., Jumadi, Saputra A. and Fikriyah V.N., Risk analysis of landslide impacts on settlements in Karanganyar, Central Java, Indonesia, International Journal of GEOMATE, Vol. 19, Issue 73, 2020, pp. 100-107.
[19] Tsuda H., Proposal for a new method on slope failures survey by AHP, Landslides – Journal of the Japan Landslide Society, Vol. 36, Issue 1, 1999, pp. 4-11 (in Japanese).
[20] Miyagi T., Prasad G.B., Tanavud C., Potichan A. and Hamasaki E., Landslide risk evaluation and mapping -Manual of aerial photo interpretation for landslide topography and risk management-, Report of the National Research Institute for Earth Science and Disaster Prevention, No. 66, 2004, pp. 1-137.
[21] Yagi H., Higaki D. and JLS Research Committee for Detection of Landslide Hazardous Sites in Tertiary Distributed Area, Methodological study on landslide hazard assessment by interpretation of aerial photographs combined with AHP in the middle course area of Agano River, Central Japan, Landslides – Journal of the Japan Landslide Society, Vol. 45, Issue 5, 2009, pp. 358-366 (in Japanese).
[22] Pourghasemi H.R., Pradhan B. and Gokceoglu C., Application of fuzzy logic and analytical hierarchy process (AHP) to landslide susceptibility mapping at Haraz watershed, Iran, Natural Hazards, Vol. 63, Issue 2, 2012, pp. 965-996.
[23] Hasekioğullari G.D. and Ercanoglu M., A new approach to use AHP in landslide susceptibility mapping: a case study at Yenice (Karabuk, NW Turkey), Natural Hazards, Vol. 63, Issue 2, 2012, pp. 1157-1179.
[24] Kayastha P., Dhital M.R. and Smedt F.D., Application of the analytical hierarchy process (AHP) for landslide susceptibility mapping: A case study from the Tinau watershed, west Nepal, Computers & Geosciences, Vol. 52, 2013, pp. 398-408.
[25] Kohno M. and Maeda H., Experiment on landslide hazard mapping, based on AHP method, in consideration of point load strength of hydrothermally altered rock: -Example in the Ohekisawa-Shikerebenbetsugawa landslide area, Japan-, Landslides – Journal of the Japan Landslide Society, Vol. 50, Issue 3, 2013, pp. 121-129 (in Japanese).
[26] Kil S.-H., Lee D.K., Kim J.-H., Li M.-H. and Newman G., Utilizing the analytic hierarchy process to establish weighted values for evaluation the stability of slope revegetation based on hydroseeding applications in South Korea, Sustainability, Vol. 8, Issue 1, 2016, 58.
[27] Zhang J. He P., Xiao J. and Xu F., Risk assessment model of expansive soil slope stability based on Fuzzy-AHP method and its engineering application, Geomatics, Natural Hazards and Risk, Vol. 9, Issue 1, 2018, pp. 389-402.
[28] Kohno M., Noguchi T. and Nishimura T., Landslide hazard mapping in the Chugoku Region using AHP method and GIS, Japan-, Landslides – Journal of the Japan Landslide Society, Vol. 57, Issue 1, 2020, pp. 3-11 (in Japanese).
[29] Isozaki Y., Maruyama S., Aoki K., Nakama T., Miyashita A. and Otoh S., Geotectonic subdivision of the Japanese Islands revisited: Categorization and definition of elements and boundaries of Pacific-type（Miyashiro-type） Orogen, Journal of Geography, Vol. 119, Issue 6, 2010, pp. 999-1053 (in Japanese).
[30] Satty T.L., The Analytic Hierarchy Process, McGraw-Hill Int. Book Co., New York, 1980, pp. 1-287.
[31] Geospatial Information Authority of Japan (GSI), Digital Elevation Model (DEM10B), https://fgd.gsi.go.jp/download/menu.php (in

Japanese), Accessed April 2020.
[32] Geological Survey of Japan, National Institute of Advanced Industrial Science and Technology (AIST), Seamless Digital Geological Map of Japan (1:200,000), https://gbank.gsj.jp/ seamless/ (Basic version, data update date: 29 May, 2015) (in Japanese), Accessed April 2020.
[33] Biodiversity Center of Japan, The Natural Environmental Information GIS, https:// www. biodic.go.jp/trialSystem/top_en.html (in Japanese), Accessed April 2020.
[34] Suzuki T., Introduction to Map Reading for Civil Engineers Volume l -Geomorphological Basis for Map Reading-, Kokon Shoin, Publishers, Tokyo, 1997, pp. 1-200.
[35] Tarboton, D., Terrain Analysis Using Digital Elevation Models, http://hydrology.usu.edu/ taudem/taudem5/, Accessed April 2020.